Deep Underground Neutrino Experiment (DUNE)

DUNE Near Detector
Updated Conceptual Design Report

SAND Chapter

March 26, 2024

The DUNE Collaboration

Contents

List of Figures

List of Tables

Todo list

Chapter 1

System for on-Axis Neutrino Detection (SAND)

1.1 Introduction and Overview

Near detectors (NDs) complex [2] must operate in high-rate environment. It is devoted to:

- predict the spectrum of the neutrino beam at far detector (FD),
- transfer the measurements to FD,
- constrain the cross section models,
- measure the neutrino flux,
- perform measurements with different fluxes,
- monitor variations of the neutrino beam

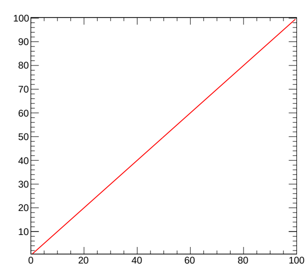

Figure 1.1: Dummy - Here insert the caption.

1.1.1 Physics Motivations

Contribution of System for on-Axis Neutrino Detection (SAND) in the Deep Underground Neutrino Experiment (DUNE) scientific plan, specifically in the ND complex ...

A component of the ND complex must remain on-axis where beam monitoring is most sensitive and collects a sufficient number of ν_μ charged current (CC) interactions.

The ND must monitor on-axis spectrum and position information to detect representative changes in the beam line.

The ND must measure external backgrounds, which include cosmic and beam-induced activity.

1.1.2 Requirements

- Statistics of ν_μ CC events. Collection and identification of enough ν_μ CC interactions to perform beam monitoring on a weekly basis (mass > 20 tons for reconstruction of p_μ, mass > 5 tons for reconstruction of E_ν);
- E_ν, p_μ resolution sufficient to detect spectral variations in ν_μ CC events from a representative set of variations on a week: $\sigma(p_\mu)/p_\mu < 10\%$ at 5 GeV/c improving at 5% at 1 GeV/c, or $\sigma(E_\nu)/E_\nu < 15\%$;
- Vertex reconstruction with a resolution < 5 cm to distinguish interactions occurring over distances where the spectrum may vary;
- Track timing. SAND must have timing to identify and select activity occurring within the neutrino beam delivery window: $\sigma_t < 5$ ns in the tracker, $\sigma_t < 400$ ps on electromagnetic calorimeter (ECAL) hits. Better resolution (1 ns) would further enable directionality capabilities.

1.1.3 Opportunities for SAND

- Cross sections ($\nu - H$, $\nu - Ar$)...
- Search for Heavy Neutral Leptons...

1.1.4 Setup

Main elements of SAND, synthetic description ...

1.1.5 Simulated Performance

1.1.6 Background Removal

1.2 Lead/Scintillating-Fiber Calorimeter (ECAL)

1.2.1 ECAL Design and Structure

The K-LOng Experiment (KLOE) ECAL [3] is a fine sampling lead-scintillating calorimeter with photomultiplier tube (PMT) readout. The central part (barrel) approximating a cylindrical shell of 4 m inner diameter, 4.3 m active length and 23 cm thickness ($\sim 15\ X_0$), consists of 24 modules with trapezoidal cross-section and fibers running parallel to the cylinder axis. Two endcaps close the barrel hermetically. Each of them consists of 32 "C" shaped modules arranged vertically along the chords of the circle inscribed in the barrel (see Fig. 1.2). In the endcap modules fibers run perpendicular to the cylinder axis, so that for the whole ECAL fibers are mostly transverse to the particle trajectories.

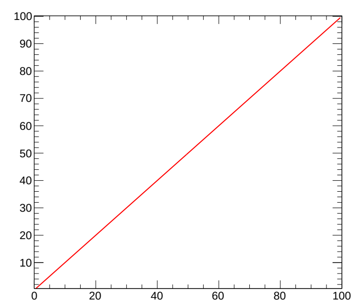

Figure 1.2: Example - Here insert the caption

The modules are read out on the two sides through Plexiglas light guides optically coupled to fine mesh PMTs. The readout granularity is $\sim 4.4 \times 4.4$ cm^2. Each barrel module has 60 channels per side while endcap modules have 10, 15 or 30 channels per side depending on their width. The total number of readout channels is 4880. Both in the barrel and in the endcaps, PMT axes are almost parallel to the magnetic field, in order to decrease the field effects on PMT response, and to increase hermeticity (see Fig. 1.2).

The basic calorimeter structure consists of an alternating stack of 1 mm scintillating fiber layers glued between thin grooved lead foils, obtained by passing 0.5 mm thick lead foils through rollers of a proper shape. The grooves in the two sides of each foil are displaced half a pitch, so that fibers are located at the comers of adjacent, quasi-equilateral triangles, resulting in an optimal and uniform arrangement of the fibers in the stack. The final composite has a fiber : lead : glue volume ratio of approximately 48 : 42 : 10, a density of ~ 5 g/cm^3 and a radiation length X_0 of ~ 1.6 cm, is self-supporting and can be easily machined. The energy sampling fraction is $\sim 18\%$ for a minimum ionizing particle (MIP) and the efficiency for low energy photons is high due to the very small lead foil thickness ($< 0.1\ X_0$).

1.2.1.1 Scintillating Fibers

Two types of fibers (Kuraray SCSF-813 and Pol.Hi.Tech. 0046) with a total length of 15.000 km have been used to assembly the ECAL. The former have higher light output and longer attenuation length, the latter are less expensive. Anyway the performance differences are not significant and the Kuraray fibers are used in the inner half of the calorimeter. All fibers have an attenuation length between 3 and 5 m and produce ~ 1 photoelectron for 1 mm of crossed fiber at a distance of 2 m from PMT. The emitted light is in the blue-green region ($\lambda_{peak} \sim 460$ nm).

1.2.1.2 Photomultipliers (PMTs)

The PMTs must operate in a magnetic field with the suitable efficiency, linearity, timing resolution and dynamical range. The Hamamatsu R5946/01 1.5' tubes have been chosen because the electron multiplication occurs between dynodes made of fine mesh, very close to each other. Then the effect of the magnetic field on the electron path is very small. Furthermore housing boxes with double mu-metal shielding reduce the field to less than 0.2 T and the PMT alignment is such that the component transverse to the tube axis is less than 0.07 T. It has been measured that the PMT gain decreases by 10% when the field is on, but linearity and resolution are not affected.
The PMTs are operated with grounded cathodes in order to eliminate leakages, possible origin of noise and field distortions. A box holds the PMT mechanically in place and a spring pushes gently it against the light guide. The optical contact PMT-light guide is made by means of Bicron optical gel BC-630. The cables are in the box and carry high and low voltage, a test pulse and the output signal.

1.2.1.3 Silicon photomultipliers (SiPMs) as Possible Spare for PMTs

The SiPMs work efficiently in a range compatible with the typical wavelength-shifted light of the scintillating fibers, and are insensitive to magnetic fields, unlike PMTs. In addition, since SiPMs operate at low voltage, the high voltage power supply would no longer be required, with convenience in compactness and cost.
For the aforementioned reasons, the substitution of PMTs with SiPMs in the SAND calorimeter, with a possible improvement of efficiency and timing resolution, has been investigated [4]. The SiPMs used in this test are the 4×4 arrays of the Hamamatsu S13361-3050 series. Anyway, it is excluded to substitute the single PMT channel with 16 readout channels. Thus, in these measurements, the SiPM array is considered as a unique element. The MPPC series has been chosen since it achieves the maximum Photo-Detection Efficiency (PDE_{MAX}) close to the peak wavelength of the scintillating fibers (typically $\mathrm{PDE}_{MAX} = 40\%$ at $\lambda = 450$ nm). But the quantum efficiency of the Hamamatsu R5946 1.5' mesh photomultiplier presently used in the calorimeter is 23% at $\lambda = 390$ nm.
A block ($24.5 \times 13.5 \times 40$ cm^3) of the lead-scintillating fiber calorimeter has been equipped (Fig. 1.3) with light guides like in KLOE. These light guides are shaped to cover the PMT surface and are not optimal for the smaller SiPM surface. Excluding the option to remove the present light guides and to mount new ones in the calorimeter, the test has been performed gluing a small adapter on the light guide to optimize the coupling with the SiPM (Fig. 1.3, right).

The signals induced by cosmic muons have been collected on one side by SiPM and on the opposite one by standard KLOE PMT. This setup allowed to compare directly the different performance. The measurements were performed for two SiPMs and two PMTs. The average results for efficiency and timing resolution in these conditions are reported in Table 1.1. Even if the differences are small, PMTs perform better in the present setup. The difficulties in coupling SiPMs with the light guides without deep mechanical changes, the lack of improvement, the cost, and the necessary commissioning time advise against the substitution of 4880 available and tested PMTs with new SiPMs. Nevertheless, the results from this study do not exclude the use of SiPMs as a spare. A

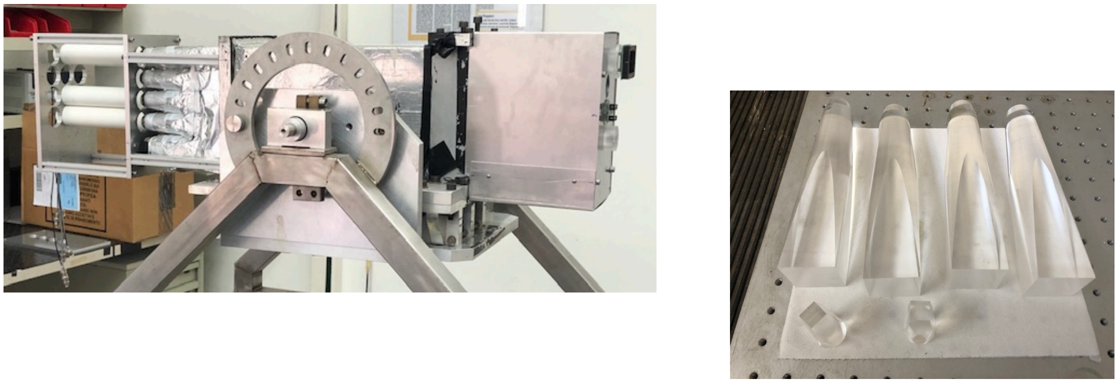

Figure 1.3: Left: experimental setup to compare PMT and SiPM. The SiPMs are on the right, the calorimeter block is at the center, the PMTs are on the left. Right: light guides and adapters for SiPM.

mechanical setup is under study.

Table 1.1: Comparison of SiPM performance with PMT ones

	Efficiency (%)	Time Resolution (ps)
PMT	91.6 ± 0.2	197 ± 4
SiPM	90.8 ± 0.3	240 ± 3

1.2.2 Performance in KLOE and KLOE-2 Experiments

1.2.3 Requirements for DUNE ND

1.2.4 ECAL Calibration and Monitor System

Ideas to calibrate SAND ECAL according to KLOE experience
Cosmic muon detection with a dedicated trigger (no beam time)

1.2.5 ECAL Electronics

PMT saturation and measurement range
picoTDC
custom board

1.2.5.1 Frontend

1.2.5.2 Data acquisition (DAQ)

1.2.5.3 High-voltage

The Hamamatsu R5946/01 PMTs require a maximum supply power of 2.3 kV, absorbing an average anode current of 0.01 mA. The CAEN SY4527 mainframe is capable of hosting up to 16 HV A7030P modules suitable for powering the ECAL PMTs. The CAEN A7030P is a module able to independently control up to 48 channels, with an output range of 3 kV/1 mA (1.5 W) at a low ripple (<20 mVpp-max in the range 10 ÷ 1000 Hz and <10 mVpp-max over 1000 Hz). The A7030P module is supplied with a high density multipin Radiall 691803004 connector. This connector is inadequate for powering the ECAL PMTs, therefore a multipin to SHV adapter will be used. The CAEN R648 19" rack module fits one Radiall 691803004-type multipin connector into 48 Radiall R317580-type SHV connectors, suitable for powering the ECAL PMTs. Moreover this module provide Interlock and Shield connections (through LEMO connectors). The described system includes a complete set of software tools for remote control (*via* Gigabit Ethernet or Wi-Fi) of both the mainframe and high voltage boards, from low-level libraries to graphical application software. Furthermore a proprietary software introduces logging capability to the system. Through this tool it is possible to records every command sent to the system and every warning/alarm detected by the system. In this way it is possible to automatically monitor the behavior of every single parameter during operations.

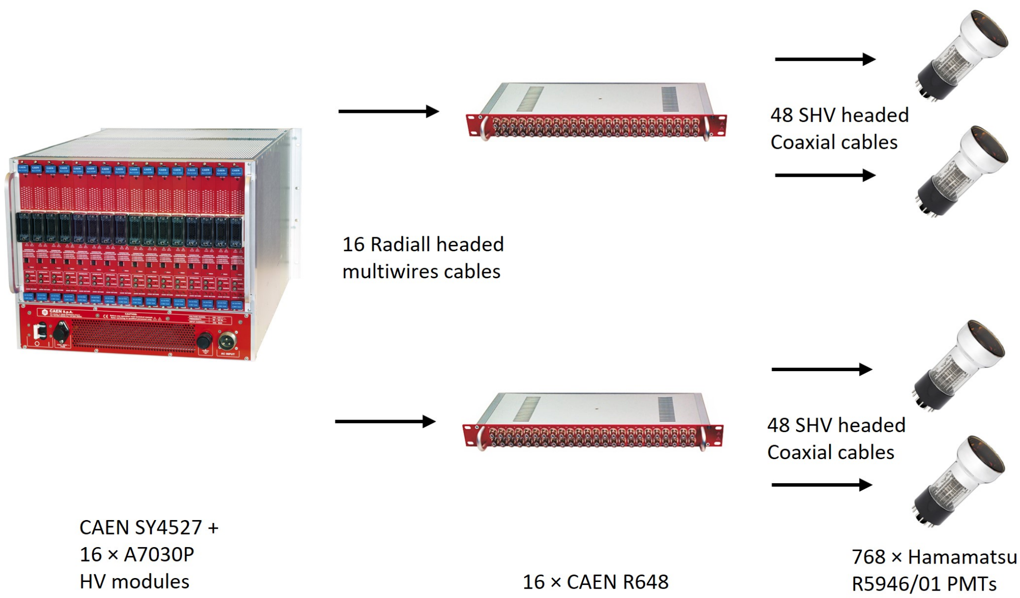

Figure 1.4: HV system to power 768 ECAL PMTs. To power all the PMTs 7 of this systems must be used.

Powering 4800 PMTs requires 100 CAEN A7030P HV modules that will be host in 7 CAEN SY4527 mainframes. In addition, 100 CAEN R648 Radiall to SHV connector adapters will be used to transfer HV power from HV module to PMTs. The unused mainframe slots can be used to save HV spare modules (Fig. 1.4).

1.2.5.4 Low-voltage

1.2.6 ECAL Dismounting Procedures

The first step to dismount the KLOE detector was the removal of cables, racks and other stuff in the experimental hall. A huge quantity of cables were unplugged from the calorimeter and the ancillary devices. Only signal and HV cables were stored to be reused ad Fermi National

Accelerator Laboratory (Fermilab). Twelve boxes were filled with 4880 signal cables and 4880 HV ones. Both the types of cables are 15 m long. From the six platforms aside KLOE 32 FEE+HV racks, 150 crates, and 3000 boards were removed.

The extraction of the Drift Chamber (DC) was the second step. Event though it will not be reused at Fermilab, the extraction was very careful because it will be displayed in the Laboratori Nazionali di Frascati (LNF) exhibition area. The DC structure is made of carbon fibers, the spherical endplates (EPs) are kept apart by 12 rods, and an external ring is coupled to each EP through 48 screws, to allow the recovery of the EP deformation under the wire tension load. The gas sealing of the chamber is ensured by the inner cylinder and 12 panels. About 60.000 wires are tensioned between the EPs, each of which is crimped on the copper feed through. The chamber extraction procedure has been thought considering several aims: to preserve the DC integrity, to avoid the wire breaking, and to ensure the safety of people.

The extraction of the DC was based on the insertion of a beam (Fig. 1.5, right) on the axis of the cylindrical chamber, its clamping on the endplates and the extraction of beam and chamber as a unique piece. More in detail, at the beginning the beams (HEA200, 6 and 5 m long) were placed on 3 reinforced concrete pillars. Then the 6-m beam was inserted inside the DC. The beam and the DC were lifted up of few millimeters by means of the crane. This was enough to unload the DC weight from the static supports inside the calorimeter. A system with trolleys, suitably positioned on the endplates, allowed the DC to slide along the beam. Once the chamber was extracted from the calorimeter (Fig. 1.5, left), it was lifted, with a suitable sling bar, and placed on a handling trolley placed at the entrance of the experimental hall. Then it was ready to be taken away.

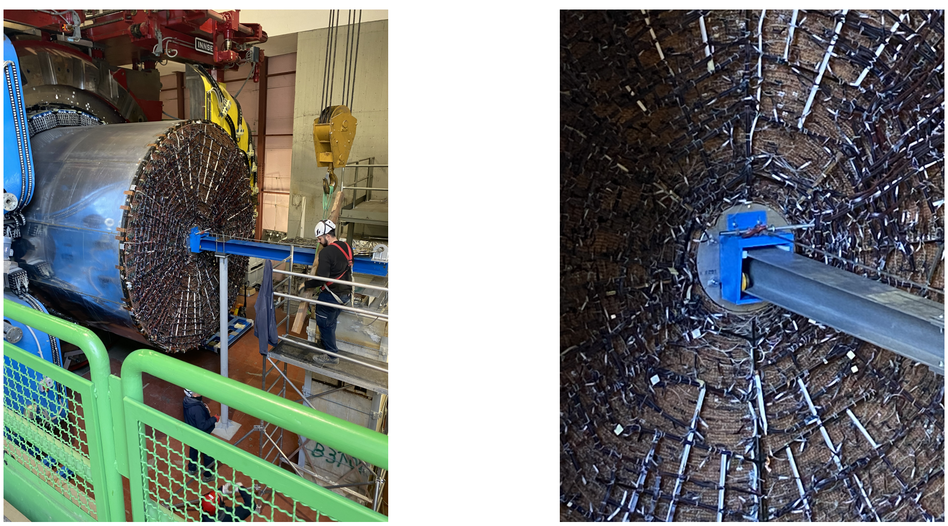

Figure 1.5: Left: extraction of the drift chamber at LNF. Right: zoom on the HEA200 beam and the trolley (detail in the text).

The dismounting of the modules of the calorimeter barrel required the construction of proper tools. These tools will be useful also in the mounting of SAND at Fermilab...

1.2.6.1 Barrel Modules

1.2.6.2 Endcap Modules

1.2.7 ECAL Revamping and Test before SAND Installation

1.2.7.1 Module Tape Re-wrapping

1.2.7.2 Light Tightness and Tests with Cosmic Rays

1.2.8 ECAL Installation & Integration

1.2.8.1 Packaging and Shipping

1.2.8.2 Storage at Fermilab

1.2.8.3 Mounting in the ND Hall

1.2.8.4 Cabling in the Alcove

1.2.9 Commissioning

1.2.10 Schedule and Milestones

1.3 The Superconducting Magnet

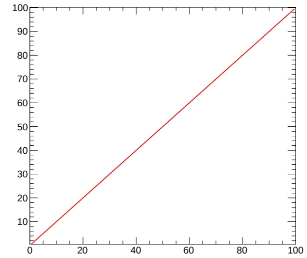

Figure 1.6: Dummy - Here insert the caption.

1.3.1 Magnet Specification

- Experimental requirements ...
- Coil parameters (operation current, stored energy ...)
- Nominal magnetic field map ...

1.3.2 Magnet Maintenance and Revamping Options

- Status
- Subsystems and components maintenance
- Obsolete or aged subsystems and components to be replaced
- New power supply (CAEN ELS)
- Power Electronics (OCEM)
- Quench detector (?)
- Control system

1.3.3 Activities at LNF

- Procurement of the cryogenic systems and materials for magnet cool down
- Magnet full operational test (full support for test/dismount/remount by ASG ?)
- Coil cool-down
- Magnet energizing test
- Coil Cryostat extraction
- Magnet turret removal
- Dismounting of Iron Yoke
- Tools, Packaging & Shipping to Fermilab

1.3.4 Installation & Integration at Fermilab

- details about the storage at Fermilab ...
- tools and mounting procedure ...
- switch-on test at Fermilab ...
- commissioning in the alcove ...
- cryogenic refrigeration plant for continuous operation of the magnet

- risk management ...
- schedule and milestones ...

1.4 LAr Active Target (GRAIN)

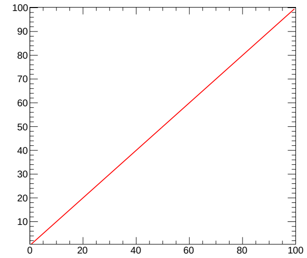

Figure 1.7: Dummy - Here insert the caption.

1.4.1 Introduction and Physics Requirements

goals for enhancing SAND capability
general requirements for neutrino event reconstruction (tracking, calorimetry, event identification)
general description of the geometry and optical detectors

1.4.2 Mechanical Design

details of inner vessel...**BOLOGNA now**
details of outer vessel

1.4.3 Optical Detector

1.4.3.1 Lens-based Optical Detector

Working principle description...**GENOVA now**

1.4.3.2 Coded Mask Detector

Working principle description [5]...**BOLOGNA now**

1.4.3.3 Detector Layout in GRanular Argon for Interactions of Neutrinos (GRAIN)

1.4.3.4 First Results with Detector Prototypes

1.4.4 Electronics

Application-specific integrated circuit (ASIC) requirements and design...(**now from ASIC document**)

1.4.5 Data Acquisition and Slow Control System

1.4.6 Neutrino Event Reconstruction

1.4.6.1 Algorithms for Track Reconstruction with Lens Images

LECCE now

1.4.6.2 Algorithms for Track Reconstruction with Coded Mask Images

BOLOGNA now

1.4.6.3 Calorimetric Reconstruction

1.4.6.4 Reconstruction Performances

GE-LE-BO now

1.4.7 Calibration System

1.4.8 Cryogenic System

BOLOGNA now

1.4.9 First Commissioning in Laboratori Nazionali di Legnaro (LNL)

1.4.10 Integration and Installation in SAND

1.5 Tracker

Introduction ...
Requirements and opportunities of the tracker system ...
Infrastructure...

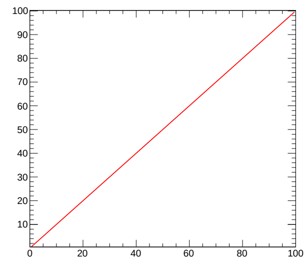

Figure 1.8: Dummy - Here insert the caption.

1.5.1 Straw tube tracker (STT)

1.5.1.1 A Compact Modular Design

1.5.1.2 Nuclear and “Solid" Hydrogen Targets

1.5.1.3 Engineering Model

1.5.1.4 Technology and Performance

1.5.1.5 System Integration

1.5.1.6 Electronic Readout

1.5.1.7 Cooling System

1.5.1.8 Data Acquisition and Slow Control

1.5.1.9 Prototyping and Tests

1.5.1.10 Gas System

1.5.1.11 Fabrication and Installation

1.5.1.12 Commissioning

1.5.1.13 Calibration and Monitoring

1.5.1.14 Detector Performance

1.5.2 Drift Chamber

- Backup tracking based on drift chambers with smaller number of channels
- Small scale prototype (30×30 cm^2)
- Beam test with larger prototype (120×80 cm^2)

1.5.2.1 Layout

1.5.2.2 Mechanics

1.5.2.3 Results and Performance

Calibration ...

1.5.3 Gas System

1.6 DAQ Architecture

Data readout in one spill (∼ 3500 Mbits)
Common logic/interfaces board connected to specific front-end board (FEB) of each sub-detector
Endpoints: GRAIN 10, STT 450, ECAL 200
Data acquisition software

This chapters describes the architecture of the Data Acquisition system, as well as the closely related Timing, Trigger and Calibration interfaces, and the runtime configuration of the Front-end (FE) electronics. Each of the SAND subdetectors implements a different architecture for their FE, but must conform to a common standard for interfacing with the DAQ, and also with the Detector Control System (DCS) and Detector Safety System (DSS) described in Sec. 1.7 and 1.8. The element of a subdetector readout system which implements one or more of these standard interfaces will be called an *Endpoint* for the respective interface. The implementation of e.g. the timing distribution, the data processing, or the configuration of the readout boards that takes place inside the Endpoint(s) or between the Endpoint(s) and any separate FEB is the responsibility of the respective subdetector and will not be discussed in this chapter.

The DAQ and the Timing system used in SAND conforms to the design implemented by the other NDs and the FDs. The design is summarized here in 1.6.1 and 1.6.2 respectively and more in depth information is available in

1.6.1 DAQ Interfaces

The requirements of SAND in terms of data volumes are modest, at least when compared with those of the FD. A summary of the amount of data produced by the subdetectors during a spill, outside of a spill, and during periodic calibration/alignment runs is shown in Table

1.6.1.1 ECAL

1.6.1.2 GRAIN

GRAIN is read out by custom ASICs mounted in cryogenic readout boards inside the cryostat, which are connected to warm interface boards on the outside. The latter are mounted four per side of GRAIN and serve as endpoints for all common interfaces.

1.6.1.3 STT

1.6.2 Synchronous Interfaces

Requirements, logic and implementation
- overview of DUNE timing system and endpoints
- timing requirements: <100 ps within each sub-detector, O(100 ps) among different sub-detectors, ∼ 1 ns alignment with the beam
- clock alignment: O(50 ps) for GRAIN, O(100 ps) for STT and ECAL
- clock jitter: < 10 ps for GRAIN, O(10 ps) for STT and ECAL
- synchronization with the beam (custom instrumentation ?)
- ∼ ns timing accuracy to disentangle the bunch structure in the spill

1.6.2.1 Trigger

1.6.2.2 Calibration

1.7 Detector Control (DCS)

The DCS has exclusive control on the SAND detector, excluding the control of the cryogenic related to the magnet which responsibility resides with the cryo-group. This control is independent of the DCS as it involves safety aspects critical for the people on site and the experiment operation.

The DCS is built on certified equipment and will require dedicated training for its maintenance. The system will be based on the Ignition system.

The monitoring data collected by the DCS will be made available to the DAQ system as a Detector status authorizing the data acquisition sequence to proceed.

A brief description of the different subsystems, and how the DCS manage them, is given in the following.

1.7.1 DCS Devices

- **Detector Power Control**: The detector power control (DPC) is composed of the power supplies that provide power to the different parts of the detector. The DCS is in charge of processing the requests from the operators, and send the commands to the power supplies. Additionally, the DCS monitors and archives the power supply parameters, such as currents, voltages, temperatures allowing an analysis of the system behavior over time. A DSS system is also implemented and connected to the DCS, displaying an alarm in case any of the configured limits is exceeded. Depending on the severity of the alarms, corrective actions may be taken automatically to protect the detector.
- **Photon Detectors**:
- **Purity Monitors**:
- **Temperature Monitors**:
- **DAQ Rack Control**: The DCS system monitors all working parameters of the water circuit and of the racks and is able to cut power if the ambient temperature raises beyond a settable threshold. It also controls the staged re-powering of racks during a cold start procedure, in order to limit the instantaneous load in the electric distribution system.
- **External Systems**: The cryogenics control system does not belong to the Detector DCS but to the Cryo DCS system. However, the DCS and the DCS cryogenics control system continuously exchange information.

1.7.2 DCS Unifying Standards

The DCS provides a homogeneous environment into which all its parts can be integrated. This environment for the DUNE-SAND experiment is depicted in Fig. 1.9.

The communication protocols used to interact with different hardware components are, in most

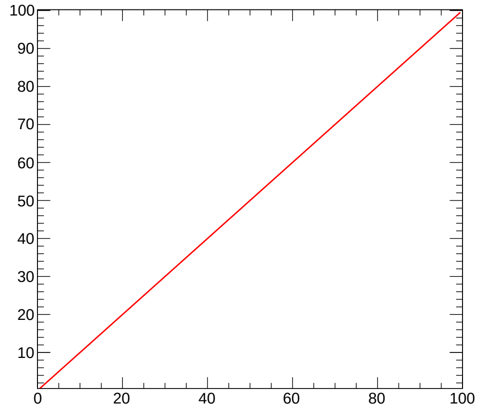

Figure 1.9: DCS preliminary layout.

cases, fixed by the manufacturers. Therefore, the DCS has to be able to support a variety of communication mechanisms and to abstract those, such that their difference is not visible to the higher levels of the supervisory system, as well as to the operators. The communication layers used within DS20k detector and their main characteristics are listed here:

- OPC classic (OLE1 for Process Control Data Access): The OPC Classic specifications are widely used in the Industry as the standard interface for hardware communication.The OPC Classic specifications provide a middleware to decouple the hardware specific elements from the software in charge of its control.
- OPC unified architecture: The OPC Unified Architecture (OPC UA) was designed to enhance and surpass the capabilities of the OPC Classic specifications. Its functionality remains the same but with several improvements that ease its operation.

1.7.3 Detector Operation

The primary challenge for the DUNE-SAND DCS was its extremely tight development and installation schedule. The DCS needed to rely on existing solutions. The software chosen to operate the DCS is a commercial supervisory control and data acquisition (SCADA) toolkit - Ignition. Ignition is based on a distributed product, where quasi-independent processes, called managers, execute different tasks. Those managers do not need to run on the same machine and may be distributed, together with the Ignition internal database, to several computers running on Linux. A critical component in the DUNE-SAND DCS is the Access Control component. With the access control enabled, every user logs in with his personal account to perform any DCS action. Three authorization levels are in use: Monitor, Operator, and Expert. Depending on the user's rights, different actions can be blocked or hidden to protect the detector integrity and to better guide the user.

Another critical interface in the DUNE-SAND DCS system is the integration with the DUNE-DAQ slow control.

In case of emergency situations the DCS will operate and control such interfaces even when the

DAQ is running.

1.7.4 Basic and Advanced Operations

The basic operation of the detector uses a simplified interface that allows to the operators a smooth execution of their tasks, minimizing unintended actions and therefore increasing the stability of the system. For monitoring purposes, the interface uses simple color coding in order to be as straightforward as possible. It is based on two main concepts:

- Dynamic objects, where all the graphical items are dynamic and thus can be used to navigate through the different parts of the detector to see its dedicated panels.
- Data widget, where the datum displayed on the DCS interface is more than a pure value and the operators may perform some extra actions such as plotting its historical values or check its status.

For advanced detector operations, specific and more details panels have been designed. Rather than using an FSM for moving the detector –or its sub-components– to a preset state, the advanced panels allow the experts, credited by the access control, the full control of the different parts of the detector. The advanced panels connect with the lowest level architecture of the detector, allowing the experts to modify operational parameters, set limits for alerts or directly control critical devices.

1.7.5 DAQ-DCS Interfaces

1.7.5.1 Calorimeter

1.7.5.2 GRAIN

1.7.5.3 STT

1.7.5.4 Magnet

Cryogenic Controls
Power

1.8 Detector Safety Systems (DSS)

The DSS is an independent safety system that interacts directly with the Cryogenics, SAND detector sub-components in order to assure the safety of the equipment and people and various power supplies.

The function of the DSS is to detect abnormal and potentially harmful situations, minimizing the resulting damage to the experimental equipment by taking protective actions in order to bring the detectors to a ”safe state“. DSS serves as an equipment protection layer between the Live Protection System (Level 3 alarms at Fermilab), which provides the highest level of safety, and the Slow Controls or Detector Control System (DCS), which performs normal operations. DCS may handle a lower level of safety.

DSS complements existing systems such as DCS or Live Protection System, and sub-detector safety systems that provide an internal sub-detector safety level are also complementary to DSS.

Based on the requirements mentioned above, the following specifications have been defined for the DSS.

- Highly reliable and available, as well as simple and robust.
- provide a cost-effective solution for experimental safety,
- operate permanently and independently of the state of DCS and Live Protections System, able to take immediate actions to protect the equipment,
- Scalable, so that it may evolve with the experiments during their assembly, commissioning, operation and dismantling (a time-span of approximately 20 years),
- Maintainable over the lifetime of the experiments,
- Configurable, so that changes in the setup can be accounted for,
- Able to connect to all sub-systems, services and sub-detector safety systems,
- To exchange information or signals with DCS and Live Protection System

1.8.1 DSS Devices

The detector safety system will be based on SIEMENS PLC architecture that will be connected directly to the DUNE-SAND power supplies as interlocks, and it will be integrated in the Ignition SCADA system as well.

1.8.2 DSS Control Hardware

DSS can adopt the standard industrial solution for critical system, by using Programmable Logical Controller (PLC) with redundant CPU in order to avoid the detector downtime The choice of the SIEMENS S7-1500H, in particular the CPU 1517H provides an optimal solution for redundancy and high availability systems.

A backup PLC CPU synchronized with the primary PLC CPU ensures that no data is lost in the switchover in case of failure. The switchover time between the failing primary CPU to the backup is less than 100 ms. The synchronization of the CPU's is made via module/optical fiber capable up to 3 km.

The PLC network uses the industrial Ethernet protocol PROFINET, connecting the CPU's with the remote extension I/O in a ring configuration. The PLC ring configuration ensures the proper functioning of the redundancy taking into account all the possible failure cases of the CPU and/or remote I/O.

The CPUs are installed in a rack called DSS CPU racks, and the remote extension I/O is also installed in the DSS Extension rack. The primary CPU is installed either on the surface or in the service cavern, while the backup CPUs are installed in the experimental cavern. Both CPUs are synchronized by means of optical fiber.

The DSS remote expansion racks are the end-points of the DSS signals. DSS signals are only connected by hardware, by means cables. The CPU's racks contains I/O modules for connecting DSS signals. External software protocols or field buses cannot connect to DSS.

- DSS can receive digital input in PLC logic level: Low = 0 V, High = 24 V
- DSS can send digital output signals with dry relay contact format
- DSS can receive analogue signals: 0-10V, 4-20mA, 0-20 mA, PT100, PT1000 type

The design of DSS signals electrical circuit is referred to as fail-safe, due to its intended design to default to the safest mode in the event of a common failure such as a broken connection in the wiring.

The size of the DSS, in other words the number of DSS Remote Expansion racks, depends of the number of signals to be processed.

DSS racks can be strategically placed in the experimental cavern in order to minimize the routing of the DSS cables.

The back-planes allocate the different DSS I/O modules; 4 types of I/O modules are used in the default configuration.

- 32 Digital Input Module
- 32 Digital Output Module
- 8 Analogue Input Module
- 8 RTD Input Module

The I/O modules are plugged into the back-plane, as shown in Figure 1.10, according to the configuration required by the application. They communicate through the back-plane with the first module, which is the Profinet communication module linked to the communication ring.

1.8.3 DSS Rack

The design of the racks is uniform for all DSS racks, maintaining the same layout and components to minimize assembly time, costs, and simplify operation and maintenance. The typical and initial hardware format of the DSS is a 19' rack with a height of 56U, but it can also be produced in other formats such as expansion mini-crates or industrial cubicles. One of the key aspects of the DSS is the power supply circuit, which needs to be highly reliable and readily available, as well as simple and robust. The DSS PLC and all associated instrumentation are powered by 24 VDC (Volts Direct Current).

The 24 VDC is generated from a reliable 220 VAC power supply.

The cables driving the signals from/to DSS PLC are physically connected to specific modules depending of the signal type.

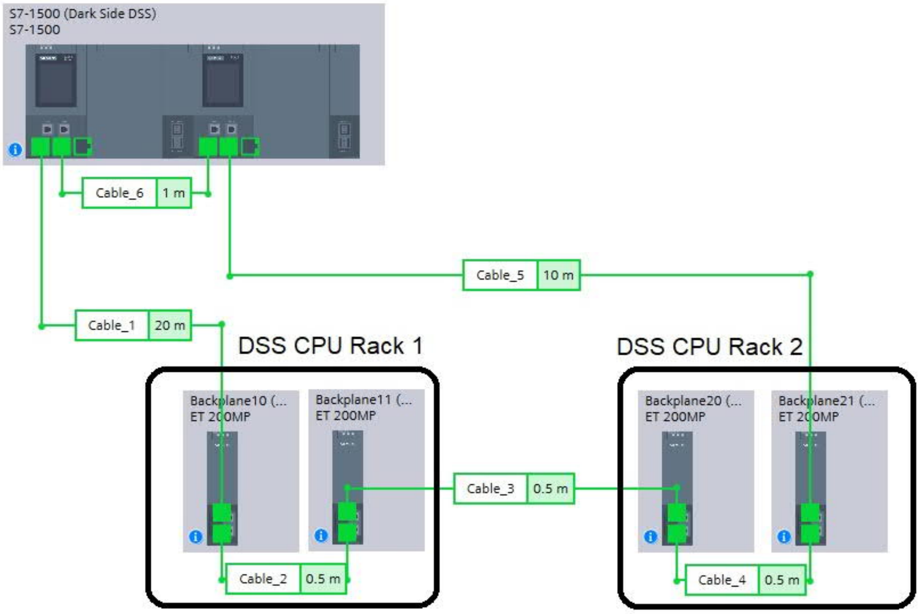

Figure 1.10: Basic layout of a DSS system with only two CPU racks: one in the service cavern and the second one in the experimental cavern. They are connected in a ring topology with the I/O back-planes to ensure redundancy. Each rack contains 2 I/O back-planes.

- The digital input signal are optocoupled and over-voltage protected for all incoming signals to DSS.
- The digital output are interfaced by using electromechanical relays in order to transmit the signals with dry relay contact.
- The analogue signals and PT100/P1000 sensors are also interfaced to the PLC module in order simplify the cable and routing.

1 # 1.9 Software and Computing

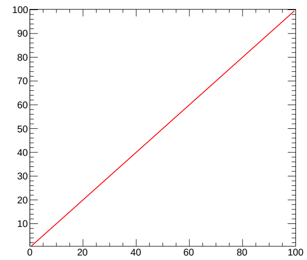

Figure 1.11: Dummy - Here insert the caption.

1.9.1 Code

1.9.1.1 Repositories

1.9.1.2 Formatting

1.9.1.3 Continuous Integration

1.9.1.4 Code Documentation

1.9.2 Simulations

1.9.2.1 Neutrino Fluxes

1.9.2.2 Geometry

1.9.2.3 Event Generator

1.9.2.4 Overlays

1.9.2.5 Particle Propagation

1.9.2.6 Detector Simulation

1.9.2.6.1 ECAL

1.9.2.6.2 GRAIN

1.9.2.6.3 Tracker

1.9.3 Reconstruction (Algorithms)

1.9.3.1 Tracker

1.9.3.2 GRAIN

1.9.3.3 ECAL

1.9.3.4 Global Event Reconstruction

1.9.4 Data Formats

1.9.4.1 Edepsim Output

1.9.4.2 Detector Simulation Output

1.9.4.3 Reconstruction Output

1.9.4.4 Common Analysis Files

1.9.5 Computing resources

1.9.5.1 Data volume

1.9.5.2 Data processing

1.9.6 Visualization

1.9.7 Integration

1.10 Event Reconstruction (Performance)

1.10.1 Single Particle Reconstruction

The reconstruction of single particles produced in neutrino interactions using the available information in the STT and ECAL detectors was firstly studied. Charged tracks are reconstructed starting from the single hits related to the energy deposited by the particle in the active gas of the straws. Figure 1.12 shows the STT hit efficiency as a function of the minimum threshold required in individual straws for muon tracks in ν_μ CC interactions. Thresholds of about 250 eV or lower are possible for tracking purpose, with a single hit efficiency >99.4%. As discussed in Sec. 1.5, the FE readout electronics is required to be sensitive down to energies comparable to the one of a single ion pair. In the following we will assume a conservative threshold of 250 eV. This value is consistent with the one used in the ATLAS TRT [6], although the VMM3 readout foreseen in STT has a lower noise level. We note that the single hit efficiency for the chosen threshold is higher for p, $e^\pm$, as well as for $\pi^\pm$ and K due to the higher average energy deposition in the straws.

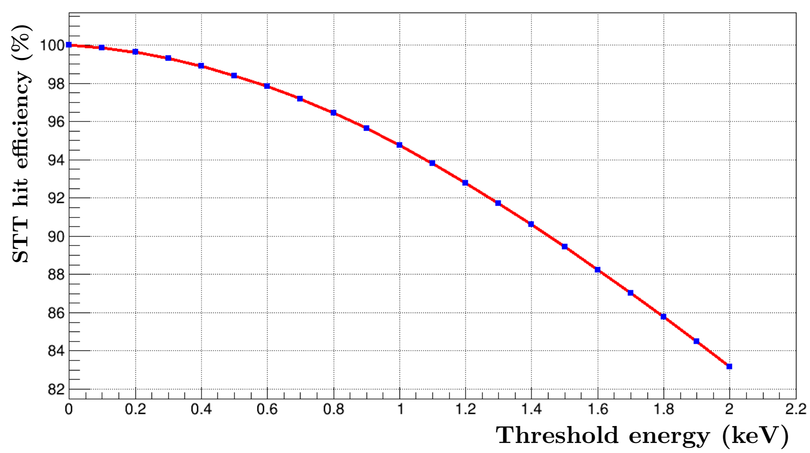

Figure 1.12: STT hit efficiency as a function of the minimum energy threshold applied to the energy detected in the active gas of the straws for muon tracks in ν_μ CC interactions. The gas mixture is Xe/CO_2 70/30 operated at an internal pressure of 1.9 atm. Results are obtained from a GEometry ANd Tracking (Geant4) simulation.

1.10.1.1 Track Reconstruction in GRAIN

Bla bla bla

1.10.1.2 Track Reconstruction in the Tracker (STT)

In order to estimate the detector performance, a simplified method for track fitting has been implemented assuming that the particle (e.g. the muon) track was well identified. The events are selected requiring at least 5 STT hits related to the track in the bending plane ($y-z$ view). This cut implies the introduction of a target fiducial volume, that is the interaction vertex must be at least 30 cm far away from the walls of the detector. The sagitta method, the parabola-fit and the circumference-fit have been tested in order to estimate the muon momentum in the bending plane (p_{yz}). The two fit methods are preferred because they exploit the large number of STT hits and the circumference-fit turns out to be the best one.

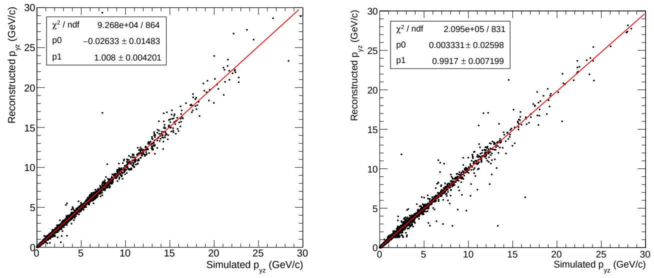

Figure 1.13: FLUktuierende KAskade (FLUKA) simulation - Scatter plot of the reconstructed muon momentum on the bending plane vs the simulated one (left: GRAIN liquid argon (LAr), right: STT target).

The track fit, then the curvature in the bending plane and the subsequent momentum estimate, can be improved by taking into account the particle energy loss and the multiple scattering in the crossed material. These effects are exploited in the fit method using the Kalman Filter.

Bla bla bla

1.10.1.3 Muon Momentum and Angular Resolutions (from STT Track)

The measurement of the muon momentum has been studied by means of two different simulation codes (Geant4 and FLUKA). Both the models corresponding to very similar results, details are given only for the FLUKA one, whereas for Geant4 just the results are depicted.

FLUKA simulation - Assuming the DUNE-neutrino beam, two different data samples have been generated. In the first sample 10^4 neutrino interactions are simulated in the LAr in GRAIN, in the second sample 10^4 neutrinos interact in the STT volume (mainly in the radiator). In both cases the muon-track reconstruction is based on the STT hits, assuming a spatial resolution of 0.2 mm on y and x axes and 0.01 mm on z axis (beam axis).

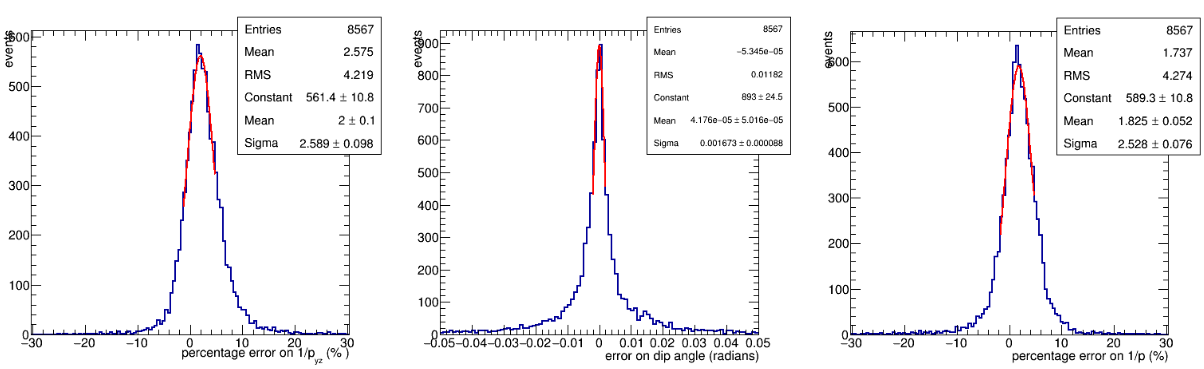

Figure 1.14: FLUKA simulation, GRAIN - Percentage errors on the muon momentum measurement: momentum on the bending plane (left), dip angle (center), momentum (right).

Then two other very loose cuts are applied looking at the fit results. One is referred to the

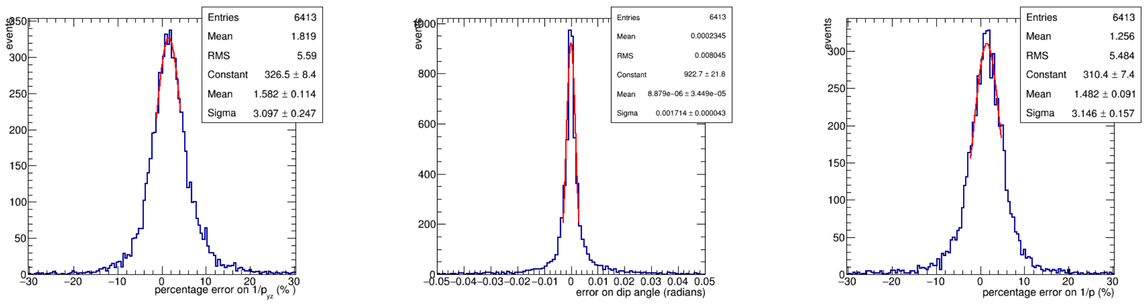

Figure 1.15: FLUKA simulation, STT target - Percentage errors on the muon momentum measurement: momentum on the bending plane (left), dip angle (center), momentum (right).

reduced-chisquare value, and the other one requires that the reconstructed Larmor radius is lower than 200 m, which implies a muon energy lower than ∼36 GeV. After the estimate of the muon momentum in the bending plane (Fig. 1.13), the dip angle (λ) is measured by the fit of the track in the $\rho - x$ plane [7]. As a conclusion the reconstructed muon momentum is $p = p_{yz}/cos\lambda$. Fig.s 1.14 and 1.15 show the percentage error on the measurement of p_{yz}, λ and p for neutrino interactions in the LAr and in the STT, respectively. In Fig. 1.16 the percentage error on p is shown for different neutrino-energy ranges. The dependence of such error on p value is finally summarized in the plots of Fig. 1.17 both for LAr and STT target interactions.

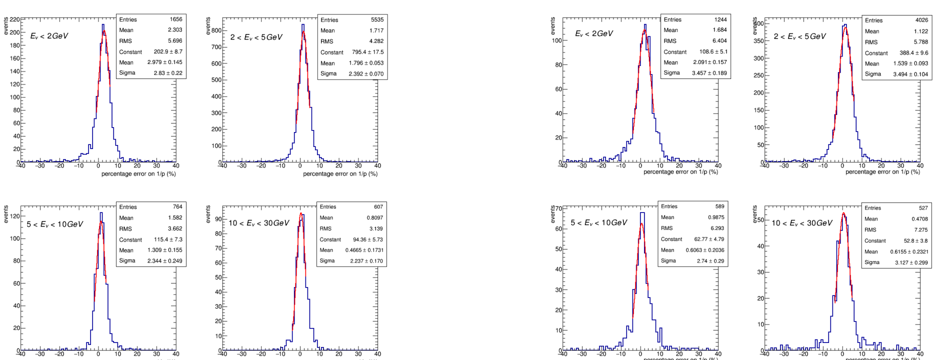

Figure 1.16: FLUKA simulation - Percentage error on the muon momentum in different neutrino-energy ranges. Left: LAr in GRAIN. Right: STT target.

In the case of GRAIN the reconstructed momentum is compared to the *true* momentum after the energy loss in LAr layer. In order to estimate the original muon momentum, the path-length and the energy loss inside LAr should be taken into account by means of the vertex reconstruction.

For both the samples (LAr and STT) the tracking algorithm can be improved by considering the energy losses in the STT volume. Up to now the algorithm has not been updated because this energy-loss effect is estimated very small.

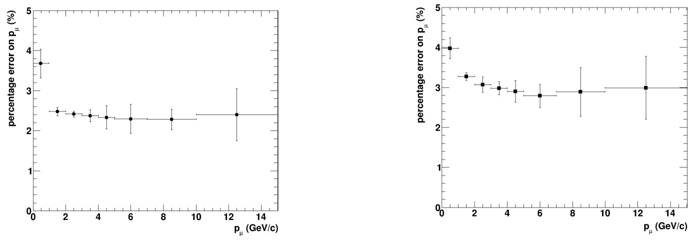

Figure 1.17: FLUKA simulation - Percentage error on the muon momentum as a function of the momentum value. Left: LAr in GRAIN. Right: STT target.

Table 1.2: Uncertainties in the reconstruction of the muon momentum.

Simulation	Target	p_{yz} (%)	dip-angle ($mrad$)	p (%)
FLUKA	GRAIN	2.6 ± 0.1	1.67 ± 0.09	2.53 ± 0.08
FLUKA	STT	3.1 ± 0.2	1.71 ± 0.04	$3.1 \pm 0.2.$
Geant4	STT	3.50 ± 0.05	1.1 ± 0.1	3.43 ± 0.05

Geant4 simulation - The results obtained with Geant4, following the *dunendggd + edep-sim* prescription, are very close to those obtained with FLUKA. The muon track reconstruction is also based on STT hits assuming a spatial resolution of 0.2 mm in the bending plane and on the same event selection described for the FLUKA simulation. Applying a circular-fit for the estimation of the muon momentum p_{yz} and a linear fit for the dip-angle λ in the $\rho - x$ plane, the total muon momentum is reconstructed. The results in terms of percentage uncertainties, as $\delta(1/p)/(1/p) = 3.4\%$, are reported in Tab.1.2.

With this simple and preliminary reconstruction, the muon charge misidentification, defined as the ratio between the number of wrong sign charges and the total number of reconstructed charges, is estimated to be 0.8% in the full momentum range.

1.10.1.4 Electron Momentum and Angular Resolutions

As for the muon performances, the electron momentum and angular resolutions has been studied by means of the two - FLUKA and Geant4 - simulations. The two codes give very similar results.

FLUKA simulation Taking into account the same fiducial volume cut on the interaction vertex - 30 cm from the walls of the detector - and applying a circular-fit model, a percentage resolution on the electron total momentum of 5.3% is obtained (Fig. 1.18, center). As stated in the previous Section, the circular-fit model does not take into account for the energy loss, and this approximation is evident in the non-Gaussian tail on the right side of the distribution shown in Fig. 1.18. This also results in a bias on the mean of 4%. The resolution on the dip-angle λ is 1 mrad with unbiased mean, the angular error distribution is shown in Fig. 1.18 (right).

With this simple and preliminary reconstruction, the electron charge mis-identification for reconstructed tracks is 1.2% in the full energy range.

Geant4 simulation The results obtained with Geant4 are compatible with those obtained with FLUKA. Following the same simulation chain used for muons (*dunendggd + edep-sim*) and applying a circular-fit model, the electron total momentum resolution is 5% with a bias on the mean of 3.8% and the angular resolution on the dip-angle is 0.8 mrad.

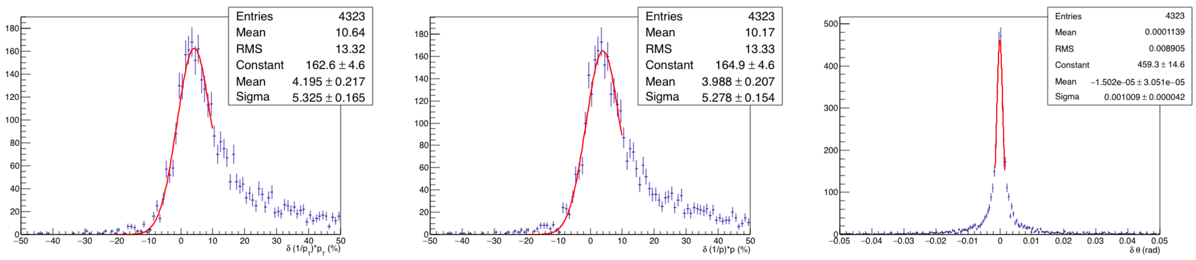

Figure 1.18: Percentage errors on electron momentum in the bending plane p_{yz} (left), on electron total momentum (center) and angular dip-angle resolution (right).

1.10.1.5 π^0 and γ Reconstruction in STT

In order to study the π^0 and γ reconstruction in STT, we simulated a sample of about 150k inclusive ν_μ CC interactions uniformly distributed throughout the STT tracking volume with Generates Events for Neutrino Interaction Experiments (GENIE)+Geant4.

The average number of π^0 produced per CC event is 0.375. Figure 1.19 shows the energy distribution of all the π^0 produced (left plot). About 1.2% of these π^0 undergo Dalitz decay $\pi^0 \to \gamma e^+ e^-$ with direct production of a e^+e^- pair. The maximal length of STT along the central diameter corresponds to about 1.34 X_0 – average density $\sim$ 0.18 g/cm^3 – and photons, on average, cross about 0.67 X_0 of material before reaching the ECAL (Sec. **??**). We therefore expect a significant fraction of the remaining γ from π^0 decay to convert into e^+e^- pairs within the STT tracking volume. Figure 1.19 shows the energy distribution for the γ converted in STT (right plot), which are relatively soft.

The average fraction of γ converting into e^+e^- pairs within the STT tracking volume is 29.2%. This number is consistent with the expectations based upon the average amount of material crossed in STT. Figure 1.20 shows the distribution of the distance traveled by the γ reaching the ECAL without converting (left plot) and the distance between the primary vertex and the conversion point for γ converting in STT (right plot). This latter distribution is relatively broad, with an average value of about 1 m. The fraction of π^0 with at least one γ converting into a e^+e^- pair within the STT tracking volume is about 49%. Events with a converted γ allow a more accurate reconstruction of the π^0, given the excellent angular and momentum resolution of STT for the e^+e^- tracks. As discussed in Sec. **??**, the large sample of converted γ available in STT will also provide a direct calibration of the electron identification and reconstruction efficiency. Figure 1.21 shows the reconstruction efficiency for the V^0 conversion $\gamma \to e^+e^-$ in the STT volume.

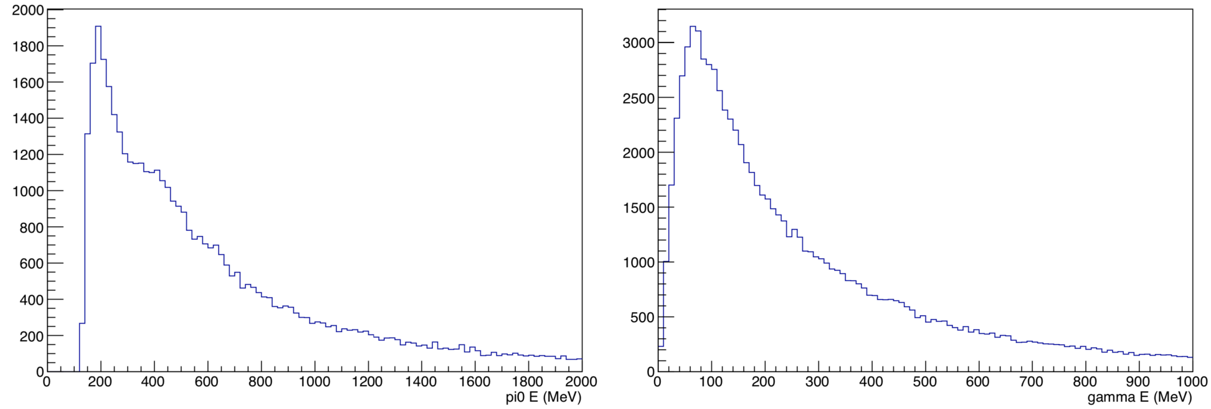

Figure 1.19: Left plot: energy spectrum of π^0 produced in inclusive ν_μ CC events with the default FHC beam. Right plot: energy distribution of γ originated from π^0 decay and converted into a e^+e^- pair within the STT tracking volume. Both distributions are obtained from GENIE+Geant4 simulations.

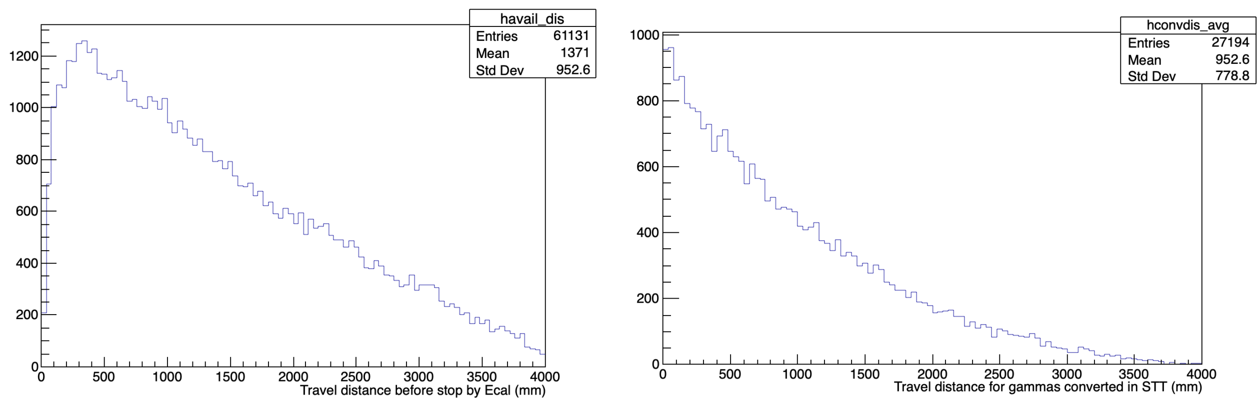

Figure 1.20: Left plot: distance traveled by the γ originated from π^0 decay before they reach the ECAL. Right plot: distance traveled by the γ from π^0 decay that convert within the STT tracking volume. The distributions are obtained from GENIE+Geant4 simulations.

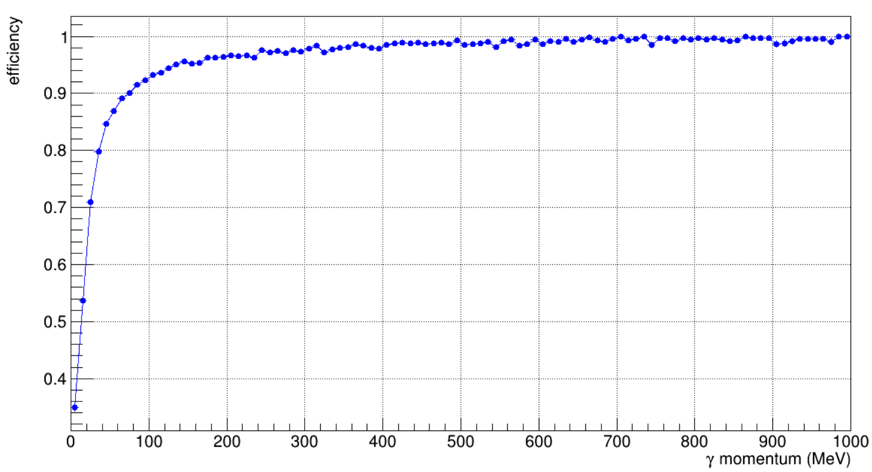

Figure 1.21: Reconstruction efficiency as a function of momentum for the conversion $\gamma \to e^+e^-$ in the STT volume. A minimum number of 4 STT hits in the YZ bending plane is required for both tracks.

1.10.1.6 Electron Momentum and Angular Resolutions (from STT Track)

1.10.1.7 π^0 and γ Reconstruction in STT

1.10.1.8 π^0 Identification and Reconstruction in ECAL

1.10.1.9 Proton Reconstruction

1.10.1.10 Neutron Detection

1.10.1.11 K^0 and Λ^0 Reconstruction

Momentum resolution and tracker target configuration ...
Acceptance and thresholds for the tracker

1.10.2 Particle Identification

1.10.2.1 Electron Identification

a. In STT
b. In ECAL ...

1.10.2.2 Proton Identification

c. from dE/dx and range
d. from time of flight (ToF)

1.10.2.3 Muon Identification

1.10.2.4 Muon/Pion Separation

e. External muon tagger

1.10.3 Neutrino Interaction Identification in the Spill

1.10.3.1 Expected Rates per Spill

1.10.3.2 Event Separation inside the Spill

1.10.4 Event Reconstruction in GRAIN

1.10.4.1 Vertex Reconstruction

1.10.4.2 Multiple Track Reconstruction

1.10.4.3 Energy Deposit Reconstruction

1.10.5 Tracker and ECAL Acceptance for Muons, Protons, Pions

1.10.6 Event Reconstruction in STT

1.10.7 Neutrino Energy Reconstruction in Inclusive CC Events

1.10.7.1 Neutrino Interaction in Upstream ECAL

1.10.7.2 Neutrino Interaction in GRAIN

1.10.7.3 Neutrino Interaction in STT

1.11 Analysis

1.11.1 Selection of CC Interactions

1.11.1.1 Kinematic Tagging of Leading CC Lepton

1.11.1.2 Selection of ν_μ & $\bar{\nu}_\mu$ CC Interactions

1.11.1.3 Selection of ν_e & $\bar{\nu}_e$ CC Interactions

1.11.2 Measurements of $\nu(\bar{\nu})$-Hydrogen Interactions

1.11.3 Determination of Relative and Absolute Fluxes

1.11.4 Constraining the Nuclear Smearing in Ar

1.11.5 ν-e Elastic Scattering

1.11.6 Coherent $\pi^\pm$ Production

1.11.7 ν_e/ν_μ & $\bar{\nu}_e/\bar{\nu}_\mu$ Flux Ratios

Low-ν relative flux...

1.11.8 On-Axis Beam Monitoring

1.11.8.1 Monitoring of the Beam Parameters

1.11.8.2 Monitoring of the Beam Direction

1.11.9 External Backgrounds

1.11.9.1 Expected Rates per Spill

1.11.9.2 Rejection of Random Neutron Background in $\nu(\bar{\nu})$-H Interactions

1.11.9.3 Rejection of Random Neutron Background in Inclusive $\nu(\bar{\nu})$ CC

1.11.9.4 Rejection of Rock Muons and Magnet Events in Upstream ECAL

1.11.9.5 Rejection of External Neutrino Interactions in STT

1.11.9.6 Pile-up Background in Upstream Barrel ECAL

1.12 Installation & Integration

Installation and integration, power, disposal ...
DOE standard, safety, logistic supply chain ...

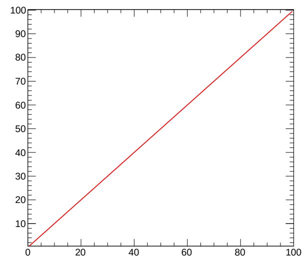

Figure 1.22: Dummy - Here insert the caption.

1.12.1 Organizational Structure and Sharing of Responsibilities

Storage area, mounting tools ...

1.12.2 Transport and Handling

Storage area ...

1.12.3 Experimental Hall and Facilities

Area (footprint) for mounting, cranes and special tooling for assembly, electrical infrastructure ...

1.12.4 Cryogenics and Gas Distribution

Area (footprint) for mounting ...
External, Proximity and Internal Cryogenics, gas system ...

1.12.5 Installation Sequence

Area (footprint) for mounting ...
Alcove area, gas system ...

1.12.6 Critical and Special Lifts

Area (footprint) for mounting ...
Alcove area, gas system ...

1.12.7 Commissioning

Sequence of operations ...

1.12.8 Safety

Applicable codes and safety infrastructure ...

1.12.9 Risk Matrix and Risk Management

Applicable codes and safety infrastructure ...

1.13 Safety

...

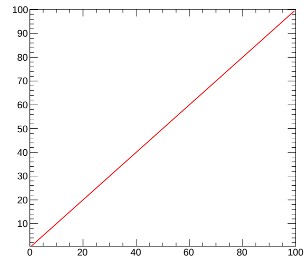

Figure 1.23: Dummy - Here insert the caption.

1.13.1 Applicable Codes and Standards

...

1.13.2 Organizational Structure

...

1.13.3 ORC List

... Operational readiness clearance (ORC) ...

1.13.4 Risk Matrices

...

Table 1.3: Dummy - An example of post-mitigation risk summary

1	ID	Risk	Mitigation	Probabil	Cost Impact	Schedule Impact
2	(id 1)	Sapien eget mi proin	Lorem ipsum dolor sit amet	L	M	L
3	(id 2)	Libero enim sed.	Urna cursus eget nunc	M	L	M
...						
n	(last id)	risk text	...	...	...	...

1.13.5 Risk Mitigation and Management

...

1.14 Organization & Management

Coordination of the groups participating in the R&D, assembling and operation of SAND is critical to successfully reach the scientific goals. Then, the SAND consortium has been created, Luca Stanco (Istituto Nazionale di Fisica Nucleare (INFN), Padua, Italy) and Claudio Montanari (INFN, Pavia, Italy) being appointed as Consortium Leader(CL) and Technical Leader (TL), respectively, by the DUNE management.

Internal boards have been setup:

- Advisory Committee (Sergio Bertolucci, Marco Pallavicini, Laura Patrizii, Roberto Petti, Milind Diwan and Bipul Buhyan)
- Steering Committee (Lea Di Noto, Matteo Tenti, Cl and TL)
- Consortium Board is foreseen but not yet defined

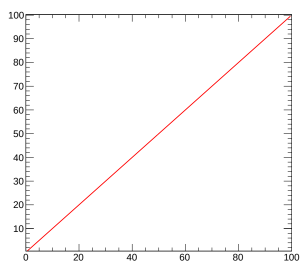

Figure 1.24: SAND consortium organizational chart.

Moreover, the consortium has been organized in Working groups (WG) related to each area of activity:

- ECAL - convenors: A. Di Domenico, D. Domenici
- GRAIN - convenors: L. Di Noto, A. Montanari
- STT - convenors: S. Di Falco, R. Petti, G. Sirri
- DAQ, trigger, timing and slow control - convenors: S. Di Domizio, C. Mariani, N. Tosi
- Physics, software - convenors: A Surdo, M. Tenti
- Calibration - convenor: P. Gauzzi

Evaluate the adequacy of the anticipated required resources
– Financial plan
– Human resources

- project organization and responsibilities
- people organization and management
- Milestones for SAND

1.14.1 Contribution by Fermilab

MoU

1.15 Time Schedule

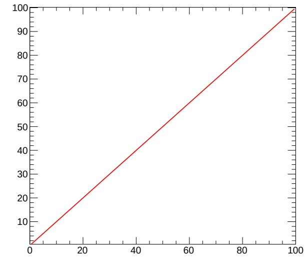

Figure 1.25: Dummy - Here insert the caption.

1.15.1 Resource-Loaded High Level Schedule

...

1.15.2 Working Groups Specific Resource-Loaded Schedules

1.15.2.1 KLOE-TO-SAND: Yoke, Magnet, ECAL

1.15.2.2 GRAIN

1.15.2.3 Tracker

1.15.2.4 DAQ, Trigger & Timing, Slow Controls

1.15.2.5 Integration, Installation and Commissioning

...

1.15.3 Milestones

...

1.15.4 Schedule-Related Risks

...

1.15.5 Schedule-Related Risk Mitigation and Management

...

Table 1.4: Example of a consortium X (fix short title, label and caption, and add your consortium items to table in chronological order among the fixed entries)

Item	Date (Month YYYY)
Start of module 0 component production for ProtoDUNE-II	(your date)
End of module 0 component production for ProtoDUNE-II	(your date)
Start of -II installation	March 2021
Beneficial occupancy of cavern 1 and central utility cavern (CUC)	October 2022
CUC counting room accessible.	April 2023
Top of #1 cryostat accessible	January 2024
End of (component 1) production	(your date)
...	...
Start of far detector module #1 TPC installation	August 2024
End of far detector module #1 TPC installation	May 2025
Top of far detector module #2 accessible	January 2025
Start of far detector module #2 TPC installation	...
End of far detector module #2 TPC installation	May 2026
...	...
last item	(your date)

1.16 Possible Upgrades

... [8]

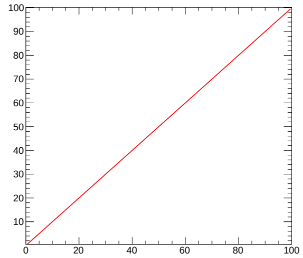

Figure 1.26: Dummy - Here insert the caption.

1.16.1 GRAIN Charge Readout

1.16.2 New Targets

Glossary

application-specific integrated circuit (ASIC) ASIC is an integrated circuit designed for a particular use. 11

charged current (CC) Refers to an interaction between elementary particles where a charged weak force carrier (W^+ or W^-) is exchanged. ii, 1, 25, 32, 33

European Organization for Nuclear Research (CERN) The leading particle physics laboratory in Europe and home to the ProtoDUNEs. (In French, the Organisation Européenne pour la Recherche Nucléaire, derived from Conseil Européen pour la Recherche Nucléaire). 44

conventional facilities (CF) Pertaining to construction and operation of buildings and conventional infrastructure, and for LBNF and DUNE project (LBNF/DUNE), CF includes the excavation caverns. 43

central utility cavern (CUC) The utility cavern at the 4850L of Sanford Underground Research Facility (SURF) located between the two detector caverns. It contains utilities such as central cryogenics and other systems, and the underground data center and control room. 40

data acquisition (DAQ) The data acquisition system accepts data from the detector front-end (FE) electronics, buffers the data, performs a , builds events from the selected data and delivers the result to the offline . ii, 5, 15–18, 37, 39, 43, 45

Detector Control System (DCS) The system devoted to .... ii, iv, 15–19

dual-phase (DP) Distinguishes one of the DUNE far detector technologies by the fact that it operates using argon in both gas and liquid phases; sometimes called double-phase. 44

Detector Safety System (DSS) Independent system interacting directly with the Cryogenics, SAND detector sub-components in order to assure the safety of equipment, people, and various power supplies. ii, iv, 15, 16, 18–21

Deep Underground Neutrino Experiment (DUNE) A leading-edge, international experiment for neutrino science and proton decay studies. 1, 15–17, 19, 43–45

electromagnetic calorimeter (ECAL) A detector component that measures energy deposition of traversing particles (in the near detector conceptual design). i, ii, 2, 3, 5, 6, 8, 15, 23, 25, 31–33, 37, 39

far detector module The entire DUNE far detector is segmented into four modules, each with a nominal 10 kt fiducial mass. 40, 45

far detector (FD) The 70 kt total (40 kt fiducial) mass liquid argon time-projection chamber (LArTPC) DUNE detector, composed of four 17.5 kt total (10 kt fiducial) mass modules, to be installed at the far site at SURF in Lead, SD, USA. 1, 15, 44, 45

front-end (FE) The front-end refers a point that is "upstream" of the data flow for a particular subsystem. For example the single-phase (SP) front-end electronics is where the cold electronics meet the sense wires of the TPC and the front-end data acquisition (DAQ) is where the DAQ meets the output of the electronics. 15, 25, 42

front-end board (FEB) Board devoted to manage the detector signal. 15

Fermi National Accelerator Laboratory (Fermilab) U.S. national laboratory in Batavia, IL. It is the laboratory that hosts Deep Underground Neutrino Experiment (DUNE) and serves as its near site. i, iii, 6–9, 38, 44

FLUktuierende KAskade (FLUKA) FLUKA is a fully integrated particle physics MonteCarlo simulation package. 26–29

far site conventional facilities (FSCF) The conventional facilities (CF) at the DUNE far detector site, SURF. 45

GEometry ANd Tracking (Geant4) A software toolkit developed by CERN for the simulation of the passage of particles through matter using Monte Carlo (MC) methods. 25, 26, 28–30

Generates Events for Neutrino Interaction Experiments (GENIE) Software providing an object-oriented neutrino interaction simulation resulting in kinematics of the products of the interaction. 29, 30

GRanular Argon for Interactions of Neutrinos (GRAIN) Subdetector of System for on-Axis Neutrino Detection (SAND). ii, iii, 11, 15, 18, 23, 25–28, 32, 37, 39, 41

Istituto Nazionale di Fisica Nucleare (INFN) Italian institution devoted to nuclear research. 37, 44

K-LOng Experiment (KLOE) KLOE is a e^+e^- collider detector spectrometer operated at DAFNE, the ϕ-meson factory at Frascati, Rome. In DUNE it will consist of a 26 cm Pb+scintillating fiber ECAL surrounding a cylindrical open detector region that is 4.00 m in diameter and

4.30 m long. The ECAL and detector region are embedded in a 0.6 T magnetic field created by a 4.86 m diameter superconducting coil and a 475 tonne iron yoke. i, 3–7, 39

liquid argon (LAr) Argon in its liquid phase; it is a cryogenic liquid with a boiling point of 87 K and density of 1.4 g/ml. 26–28, 45

liquid argon time-projection chamber (LArTPC) A time projection chamber (TPC) filled with liquid argon; the basis for the DUNE far detector (FD) modules. 43

Long-Baseline Neutrino Facility (LBNF) The organizational entity responsible for developing the neutrino beam, the cryostats and cryogenics systems, and the conventional facilities for DUNE. 44, 45

LBNF and DUNE project (LBNF/DUNE) The overall global project, including Long-Baseline Neutrino Facility (LBNF) and DUNE. 42

Laboratori Nazionali di Frascati (LNF) Istituto Nazionale di Fisica Nucleare (INFN) laboratory in Italy. i, 7, 9

Laboratori Nazionali di Legnaro (LNL) INFN laboratory in Italy. ii, 12

Monte Carlo (MC) Refers to a method of numerical integration that entails the statistical sampling of the integrand function. Forms the basis for some types of detector and physics simulations. 43

minimum ionizing particle (MIP) Refers to a particle traversing some medium such that the particle's mean energy loss is near the minimum. 3

near detector (ND) Refers to the detector(s) installed close to the neutrino source at Fermi National Accelerator Laboratory (Fermilab). i, 1, 2, 5, 8, 15

operational readiness clearance (ORC) Final safety approval prior to the start of operation. 36

photomultiplier tube (PMT) A device that makes use of the photoelectric effect to produce an electrical signal from the arrival of optical photons. v, 3–6

ProtoDUNE Either of the two DUNE prototype detectors constructed at European Organization for Nuclear Research (CERN). One prototype implements SP technology and the other dual-phase (DP). 44

ProtoDUNE-SP The SP detector at CERN. 40

System for on-Axis Neutrino Detection (SAND) The beam monitor component of the near detector that remains on-axis at all times and serves as a dedicated neutrino spectrum monitor.

i, ii, 1–41, 43

secondary DAQ buffer A secondary DAQ buffer holds a small subset of the full rate as selected by a . This buffer also marks the interface with the DUNE Offline. 42

silicon photomultiplier (SiPM) A solid-state avalanche photodiode sensitive to single photoelectron signals. iv, v, 4, 5

single-phase (SP) Distinguishes one of the DUNE far detector technologies by the fact that it operates using argon in its liquid phase only. 43, 44

straw tube tracker (STT) Tracker in SAND. ii, iv, 13, 15, 25–33, 37

Sanford Underground Research Facility (SURF) The laboratory in South Dakota where the LBNF far site conventional facilities (FSCF) will be constructed and the DUNE FD will be installed and operated. 42, 43

time of flight (ToF) The time a particle takes to fly between two visible interactions observed in the detector. If combined with the distance traveled by the particle, for example a neutron, it can be used for energy reconstruction. 31

time projection chamber (TPC) A type of particle detector that uses an E field together with a sensitive volume of gas or liquid, e.g., liquid argon (LAr), to perform a 3D reconstruction of a particle trajectory or interaction. The activity is recorded by digitizing the waveforms of current induced on the anode as the distribution of ionization charge passes by or is collected on the electrode (TPC is also used for "total project cost"). 44

trigger candidate Summary information derived from the full data stream and representing a contribution toward forming a trigger decision. 45

trigger command Information derived from one or more s that directs elements of the to read out a portion of the data stream. 45

trigger decision The process by which trigger candidates are converted into trigger commands. 42, 45

References

[1] DOE Office of High Energy Physics, "Mission Need Statement for a Long-Baseline Neutrino Experiment (LBNE)," tech. rep., DOE, 2009. LBNE-doc-6259.

[2] A. A. Abud *et al.*, "Deep Underground Neutrino Experiment (DUNE) Near Detector Conceptual Design Report," *Instruments* **5** (2021) . https://www.mdpi.com/2410-390X/5/4/31.

[3] M. Adinolfi *et al.*, "The KLOE electromagnetic calorimeter," *Nuclear Instruments and Methods in Physics Research Section A: Accelerators, Spectrometers, Detectors and Associated Equipment* **482** (2002) 364. https://www.sciencedirect.com/science/article/pii/S0168900201015029.

[4] F. Alemanno, P. Bernardini, A. Corvaglia, G. D. Matteis, L. Martina, A. Miccoli, M. Panareo, M. P. Panetta, C. Pinto, and A. Surdo, "Study of silicon photomultipliers for the readout of a lead/scintillating-fiber calorimeter," 2024.

[5] M. Andreotti *et al.*, "Coded masks for imaging of neutrino events," *The European Physical Journal C* **81** (2021) 1011. http://dx.doi.org/10.1140/epjc/s10052-021-09798-y.

[6] E. Abat *et al.*, "The ATLAS TRT electronics," *JINST* **3** (2008) P06007.

[7] F. Ragusa, "An Introduction to Charged Particles Tracking." www.mi.infn.it/~ragusa/tracking_sns_28.05.2014.pdf.

[8] B. Abi *et al.*, "Long-baseline neutrino oscillation physics potential of the DUNE experiment," *The European Physical Journal C* **80** (2020) 978.